A redox effect on the viscosity of molten pyrolite

Ana Casas, Kai-Uwe Hess, James Badro, Michael Eitel, Donald Dingwell

Chemical Geology 642 (2023) 121816

Contents lists available at ScienceDirect

Chemical Geology

journal homepage: www.elsevier.com/locate/chemgeo

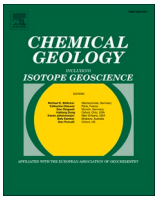

A redox effect on the viscosity of molten pyrolite

Ana S. Casas [a,b,*], Kai-Uwe Hess [b], James Badro [c], Michael Eitel [b], Donald B. Dingwell [b]

[a] Research School of Earth Sciences, The Australian National University, 142 Mills Rd., Canberra, ACT 2601, Australia
[b] Department for Earth and Environmental Sciences, Ludwig-Maximilians-Universität München, Theresienstrasse 41/III, 80333 Munich, Germany
[c] Institut de Physique du Globe de Paris, 1, rue Jussieu, 75238 Paris, cedex 05, France

ARTICLE INFO

Editor Name: Dr. Marco Fiorentini

Keywords:
Pyrolite
Mantle composition
Viscometry
Calorimetry
Fe-redox state
Levitation melting
Glass transition

ABSTRACT

The viscosity of molten Earth mantle has been determined for various redox states using very high temperature viscometry at 1 bar. The viscosity-temperature relationship of the most oxidised pyrolite studied here is comparable to that of a previous determination of the viscosity of a peridotite melt. For the first time, the effect of iron redox state on molten mantle viscosity has been determined by calorimetric analysis of the glass transition on extremely carefully characterised glassy samples quenched from conditions of variable fO_2 using gas-mixing levitation. There is a clear trend of decreasing viscosity with increasing redox state over the range of $Fe^{3+}/\Sigma Fe_{.} =$ 0.07–0.29. We also observe an increase in glass transition temperatures with increasing melt depolymerisation (i.e., higher NBO/T ratios). Both the negative oxidation dependence of viscosity and glass transition behaviour upon depolymerisation are contradictory to the trends observed from redox viscometry of more silica-rich melts but may be consistent with the broadly diminishing positive redox viscometry trends of melts with increasing basicity.

1. Introduction

Pyrolite represents a model chemical composition for the Earth's upper mantle and was initially delivered by constructing a mantle source composition for the generation of MORBs (Ringwood, 1962). Pyrolite has been a widely used model material in the investigation and constraining of the mineralogy, petrology and petrophysics of the mantle as functions of temperature and pressure (e.g., Takahashi et al., 1993; Matsukage and Kawasaki, 2014; Weidner, 1985).

The investigation of melt properties as a function of redox state has long been a component of mineral physics and experimental petrology and Fe is the major element whose redox state has been demonstrated to have significant effect on melt viscosity under terrestrial conditions of oxygen fugacity (Dingwell and Brearley, 1988; Dingwell and Virgo, 1987; Dingwell, 1991, 1995; Dingwell et al., 1988; Lange and Carmichael, 1990).

Those studies demonstrated that - for the Fe contents of natural silicate melts and their synthetic analogues - the influence of oxidation state on bulk properties (e.g., density, viscosity) is large enough to justify its quantification, parameterisation, and incorporation into models for the behaviour of high temperature molten systems within terrestrial planets. In particular, the influence of iron oxidation state on melt viscosity has been demonstrated to be broadly and nonlinearly dependent on the iron oxidation state of silicate melts such that highly oxidised melts experience a decrease in melt viscosity with reduction down to ca. 50% ($Fe^{3+}/\Sigma Fe$) followed by a near-invariance of the viscosity with further reduction (Dingwell and Virgo, 1987; Dingwell and Webb, 1990, Dingwell, 1991).

Here we present the results of a study aimed to test the effect of varying redox synthesis conditions on the viscosity of pyrolite. Using a combination of gas-mixing levitation, high-sensitivity calorimetry, and very careful glass characterisation (phase state, chemistry, and redox state) we have determined the influence of redox state on the viscosity of a synthetic molten mantle.

2. Materials and methods

2.1. Sample synthesis

A bulk sample pyrolite composition (Green, 1989) was prepared as a powder-mix of pre-dried, high purity oxide powders (SiO_2, MgO, FeO_{total}, Al_2O_3, and $CaCO_3$) weighted in stoichiometric amounts to produce pyrolite glass (Table 1). The mix was fired at 900 °C overnight for decarbonation and dehydration and pressed into a 300 mg pellet. To

* Corresponding author at: Research School of Earth Sciences, The Australian National University, 142 Mills Rd., Canberra, ACT 2601, Australia.
E-mail address: Ana.CasasRamos@anu.edu.au (A.S. Casas).

https://doi.org/10.1016/j.chemgeo.2023.121816
Received 13 April 2023; Received in revised form 26 October 2023; Accepted 6 November 2023
Available online 10 November 2023

Table 1
Bulk chemical composition of the initial pyrolite glass. Bulk chemical composition of the initial pyrolite glass.

Pyrolite starting composition		
Oxide	wt%	St dev
SiO_2	46.1	0.39
MgO	38.6	0.36
FeO_{total}	9.1	0.25
Al_2O_3	4	0.12
CaO	2.2	<0.01
Total	100	

ensure enough material was available for analysis, two batches were produced, consisting of two and four samples, respectively. 10-to-30 mg chips were broken from the pellets and loaded in the conical nozzle of an aerodynamic levitation apparatus, using a laser furnace (ALLF), where they were fused between 1900 and 2000 °C for 60 s using several Ar-CO_2-H_2 gas mixtures. The samples were then rapidly quenched to glass spheres (ranging between 1.6 and 2.2 mm in diameter) with a cooling rate of ~900 °C/s. The Ar-CO_2-H_2 gas mixture was manipulated to obtain variable fO_2 conditions for successive samples at molar mixing ratios (Ar:CO_2:H_2) ranging from 92:8:0 to 92:2.4:5.6. All fO_2 values are reported in Table 2.

2.2. Electron Probe Microanalysis (EPMA)

The major-element composition of each glass bead was determined with a Cameca SX-100 EPMA instrument of the Department of Earth and Environmental Sciences at the LMU. Pyrolite beads were prepared as epoxy-mounts, polished and carbon coated. Analysis was conducted with a 5 μm beam at 15 KeV acceleration voltage and 5 nA beam current.

Chemical homogeneity and absence of major crystalline phases in the glass were assessed by performing transect profile measurements across polished pyrolite glass sections. For each sample, two perpendicular transects composed of 17–60 spot analyses, depending on the bead size, were acquired. The standards used for calibration were albite (Si), periclase (Mg), orthoclase (Al) hematite (Fe) and wollastonite (Ca). While presence of Fe-nanolites was observed (see section 2.4), their abundance and size in all glasses were negligible in terms of bulk composition.

2.3. Bulk Fe-redox state determinations

The Fe-redox state of the samples, expressed here as ferric iron to the sum of ferric and ferrous iron ratio ($Fe^{3+}/\Sigma Fe$), was obtained by combining FeO chemical titration analyses with the electron microprobe results for Fe (total), initially cast as FeO_{total} (wt%). We applied the potassium dichromate ($K_2Cr_2O_7$) potentiometric titration method (Shapiro and Brannock, 1956; Appendix A. supplementary data), using a 665 Metrohm Titroprocessor, a 685 Dosimat automatic titrator connected to a 649 Magnetic Swing-out Stirrer with an electrode holder and a platinum reference (silver-silver) electrode. The amount of FeO (wt%) in the glasses, obtained by wet chemistry, combined with the EPMA determinations of FeO_{total} (wt%) yielded the Fe-redox state of each sample. The results are shown in Fig. 1 as a function of the gas-mixture used to synthesise the samples. These results indicate that we were generally able to quench the redox state of the high temperatures liquids in a systematic way dependent on gas-mixing induced fO_2.

The results of combined chemical characterisation, i.e., normalised major oxide concentrations, Fe-redox are summarised in Table 3. Within all pyrolite samples, the composition is constant between individual beads. The redox state varied systematically according to the gas mix employed during the levitation melting.

Table 2
Synthesis conditions for pyrolite beads. The sphere sizes L and M correspond to large (D ~ 2.2 mm) and medium (D ~ 1.6 mm), respectively.

Batch No.	Sample	Gas mixture (Ar:CO_2:H_2)	fO_2 (atm)	log fO_2	Δ IW	Sphere size
1	BAPYR19LMU1	92–8 - 0	4.85×10^{-3}	−2.31	3.8	L
2	BAPYR211LMU07–09					
2	BAPYR211LMU10–12	92–6.4 - 1.6	7.64×10^{-4}	−3.12	3.0	M
2	BAPYR211LMU13–15	92–4.0 - 4.0	1.70×10^{-5}	−4.77	1.4	M
1	BAPYR19LMU6	92–2.4 - 5.6	1.22×10^{-6}	−5.91	0.2	M
2	BAPYR211LMU16–19					

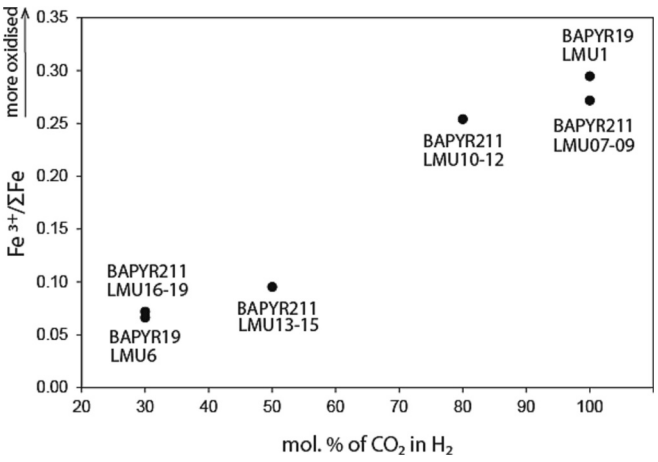

Fig. 1. Fe-redox state of pyrolite samples vs their synthesis gas-mixtures.

2.4. Magnetisation measurements

The presence and abundance of magnetic crystalline phases in the samples, prior and after DSC was determined using a 3900 MicroMag Vibrating Sample Magnetometer at the LMU. This device measures the magnetic moment of a vertically vibrating sample, which is detected and recorded by adjacent pickup coils. Results of the measurements revealed that all samples contained some crystals prior to Tg measurements and that after Tg measurements were performed, an increase in crystallinity was observed for samples synthesised under more reducing conditions; BAPYR211LMU10–12, 13–15, 16–19 and decreased for BAPYR211LMU07–09, which was synthesised under most oxidising conditions (see Fig. 2).

Determination of the magnetic crystals in the samples required measuring magnetic hysteresis loops, i.e., recording the magnetisation of the sample in dependence of the magnetic field the sample is exposed to and with respect to its magnetisation history. The chemical composition of the samples indicates that iron is the only element present in the samples that can cause a magnetic remanence; sulphur and titanium were not detected, giving rise to the conclusion that the magnetic remanence is carried by a pure iron oxide. Since the coercivity (B_C) in all the samples is low (< a few tens of mT), hematite can be excluded as a carrier of the magnetic remanence, hence we ascribe all the magnetic remanence to magnetite – before as well as after Tg measurements. The magnetic hysteresis curves are available in Appendix A. supplementary data.

Table 3
Synthesis conditions, normalised concentrations of major oxides (wt%) and $Fe^{3+}/\Sigma Fe$ ratios of pyrolite samples, produced as glass spheres.

	Synthesis gas mixture	Fe-redox state	Normalised concentrations (wt%)					
Sample	**mol.% CO_2 in H_2**	**$Fe^{3+}/\Sigma Fe$**	**SiO_2**	**MgO**	**Al_2O_3**	**CaO**	**FeO**	**Fe_2O_3**
BAPYR19 LMU1	100	0.29	46.73	37.91	4.31	2.14	6.08	2.82
St dev		–	0.39	0.3	0.12	<0.1	0.29	0.32
BAPYR211 LMU07–09		0.27	46.02	38.45	4.03	2.37	6.43	2.67
St dev		–	0.4	0.43	0.11	<0.1	0.27	0.2
BAPYR211 LMU10–12	80	0.25	45.52	38.88	3.92	2.41	6.70	2.54
St dev		–	0.52	0.44	0.27	0.11	0.3	0.26
BAPYR211 LMU13–15	50	0.09	46.39	38.32	4.09	2.41	7.85	0.92
St dev		–	0.6	0.12	0.15	0.14	0.34	0.4
BAPYR19 LMU6	30	0.06	46.87	37.88	4.32	2.15	8.12	0.64
St dev		–	0.12	0.38	0.36	<0.1	0.25	0.3
BAPYR211 LMU16–19		0.07	45.73	39.31	4.11	2.43	7.78	0.61
St dev		–	0.35	0.4	0.11	0.1	0.22	0.16

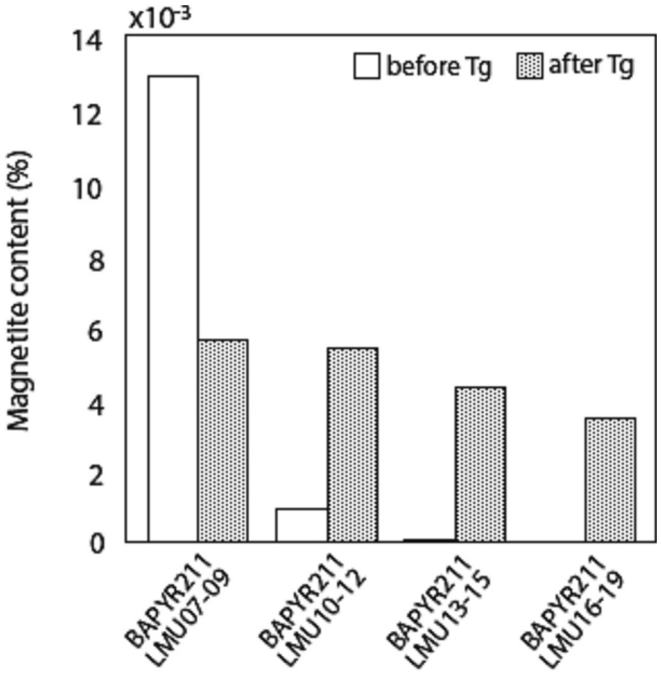

Fig. 2. Percent of magnetite (Fe_3O_4) content in samples before (white bars) and after (dotted bars) Tg measurements. Note that values on the y-axis are all elevated to 10^{-3}.

It is clear from the magnetisation results in Fig. 2 that the concentrations of magnetite determined in all glass samples, both before and after calorimetry are so low as to not have impacted the bulk chemistry or the redox state of the bulk glasses significantly.

2.5. Differential scanning calorimetry (DSC)

Differential scanning calorimetry has been performed using a Netzsch DSC 404C calorimeter at 1 bar. Samples with a weight between 6 and 12 mg were placed into a Pt-crucible (with lid) and heated in a high purity dynamic Ar (4.8) atmosphere (25 ml/min) with a heating rate of 25 K/min above the glass transition interval and cooled with a cooling rate of 10 K/min. Subsequently a (matching) heating rate of 10 K/min has been applied. Good glass transition temperature peaks have been obtained., as shown in Fig. 3. The glass transition temperature was extracted as the peak temperature, Tg_{peak}, of this run. A temperature calibration has been performed using the melting points of In, Zn, Al and Au. The corrected Tg_{peak} temperatures (where the error is ±1 °C) and the ratios of non-bridging oxygens per tetrahedral cation (NBO/T) are reported in Table 4.

The glass transition peak-temperatures (Tg_{peaks}) have been obtained under conditions of controlled heating and cooling on the products of the quenched levitation-melted samples generated in this study lie in the range of 748–740 (±1) °C. The very high precision of the calorimetric Tg determinations permits the evaluation of oxidation state on glass Tg values. Fig. 4 shows a clear shift in Tg_{peak} to lower temperature with increasing oxidation state. Furthermore, Fig. 5 further shows the effect of melt depolymerisation (i.e., increasing NBO/T ratios) on the glass transition temperature.

2.6. Viscosity measurements

The liquidus of pyrolite has been extensively investigated at high pressures but has been all but ignored at 1 bar pressure. Typical representations of the P-T path of pyrolite liquidus in the literature involve extrapolations below 1 GPa. Many of these extrapolations lie above 1700 °C which, if applicable to oxidising conditions, would preclude laboratory viscometry using our set-up. An exception to the lack of 1 bar liquidus determinations is provided by Takahashi et al. (1993) where a high temperature CO_2-H_2 gas mixing vertical tube furnace was used to obtain phase assemblages from drop quenched sample up to 1600 °C. At this temperature, the presence of olivine is noted such that the liquidus must lie (just?) above this temperature.

With the ill-constrained pyrolite liquidus (especially under oxidised conditions) in mind, we chose here to start at the highest achievable temperature of our set-up first and then to decrease the temperature stepwise in 10 °C steps until evidence from viscometry form crystallisation influences or instability were observable. For the superliquidus viscometry a separate batch of ca. 200 g was generated by mixing the pre-dried reagent-grade oxides SiO_2, MgO, FeO_{total}, Al_2O_3, and $CaCO_3$ Al_2O_3 and directly fusing the mixture in a Pt-crucible at 1675 °C in a $MoSiO_2$ Nabertherm Box Furnace for ca. 1 h. The resulting material had the following normalised composition: 46.89 (±0.39) wt% SiO_2, 37.91 (± 0.39) wt% MgO, 8.71 (±0.27) wt% FeO_{total}, 4.31 (± 0.12) wt% Al_2O_3 and 2.16 (±0.09) wt% CaO.

Viscosity was determined using the concentric cylinder technique using high temperature assembly parts exclusively composed of $Pt_{80}Rh_{20}$. The actual device used is based on the basic description of the technique provided by Dingwell (1986) and Dingwell and Virgo (1987, 1988). For this study spindle rotation speeds of 100 rpm have been achieved and the resultant torque values have been converted into viscosities using calibration coefficients extrapolated from 40 rpm. Due to the extreme operating conditions of this study, the uncertainties estimated for the current approach are larger than those typical for this technique at ±0.075 $\log_{10}$ units (c.f. Dingwell et al., 2004).

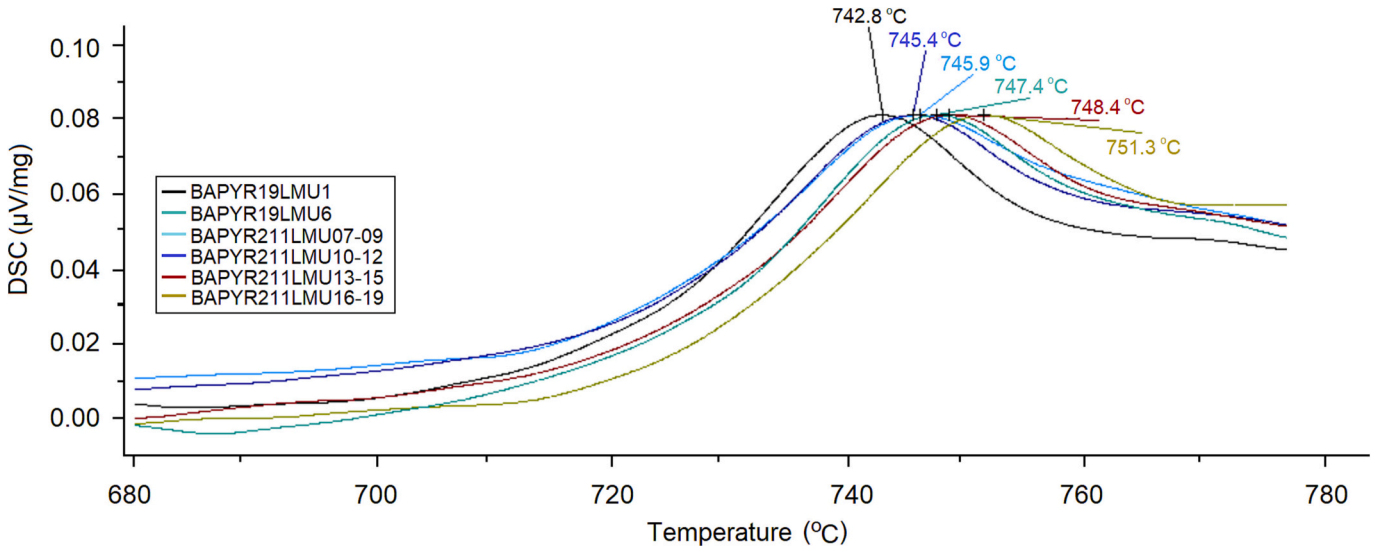

Fig. 3. Glass transition peak temperatures obtained by DSC analysis.

Table 4
Glass transition peak temperatures and NBO/T values of pyrolite quenched melts. Error is ±1 °C for Tg_{peaks}.

Sample	Weight (mg)	Tg_{peak} (°C)	NBO/T
BAPYR19LMU1	11.45	740	2.23
BAPYR19LMU6	8.89	744	2.39
BAPYR211LMU07–09	7.97	743	2.34
BAPYR211LMU10–12	12.16	742	2.41
BAPYR211LMU13–15	9.22	745	2.44
BAPYR211LMU16–19	6.64	748	2.54

The superliquidus viscosity determinations are presented in Table 5 as well as in Fig. 6, as a function of reciprocal absolute temperature.

3. Results

3.1. Calorimetrically derived subliquidus viscosity

The relaxation of enthalpy being recorded in scanning calorimetry is intimately linked to the relaxation of shear stress defining viscosity through the structural relaxation of the supercooled liquid state at the glass transition (Stevenson et al., 1995). Using the concept of a shift factor relating shear viscosity to the temperature at the glass transition peak (Ferry, 1980; Rongzhi, 2000), we can assign viscosity values to the Tg values presented in Table 5 (using the shift factor employed by Dingwell et al., 2004; resulting in a common viscosity of log 10.43 (Pa s)

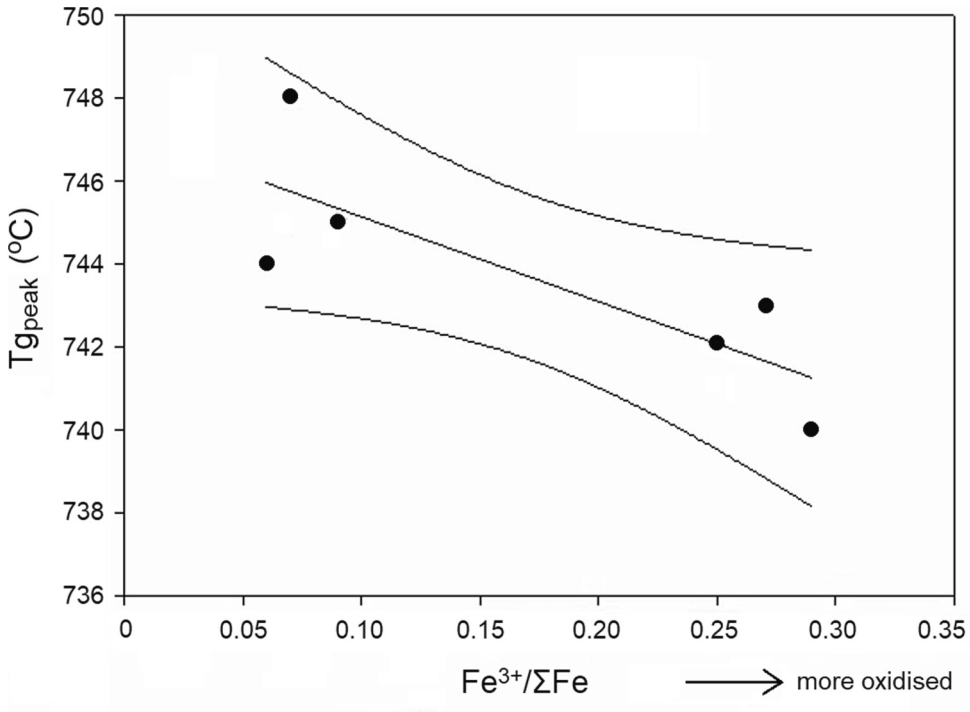

Fig. 4. Tg_{peak} vs Fe-redox state of pyrolite quenched melt. Both heating and cooling rates were at 10 °C/min. Upper and lower lines are 95% confidence intervals.

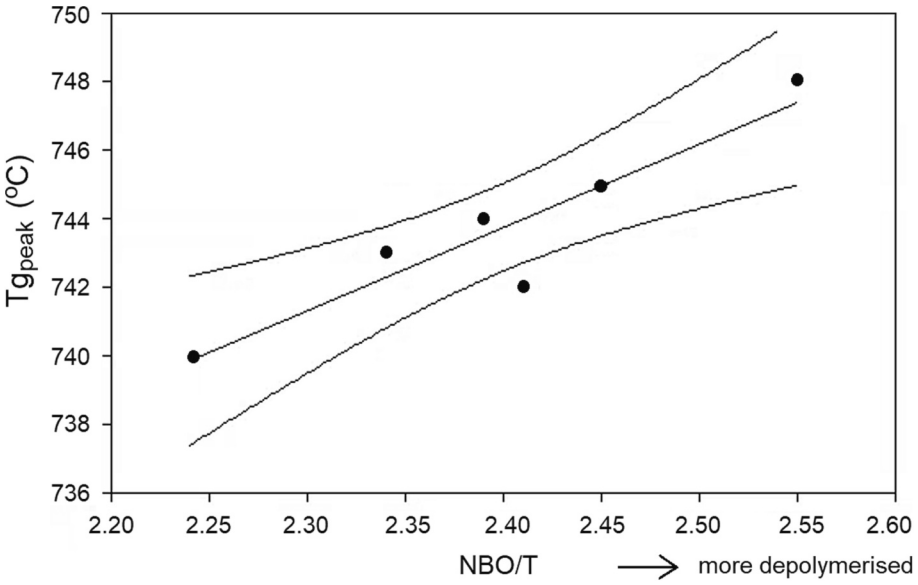

Fig. 5. Tg_{peak} vs the ratio of non-bridging oxygens per tetrahedral cation (NBO/T), which is a measure of the degree of polymerisation in melts. Upper and lower lines are 95% confidence intervals.

Table 5
Superliquidus viscosity (η) data.

T (°C) nom.	T (°C) calib.	10^4/T (K)	torque %100 rpm	η Pa·s	log η Pa·s
1670	1664	5.162	3.044	0.085	−1.072
1660	1654	5.189	3.129	0.087	−1.060
1650	1644	5.216	3.220	0.090	−1.047
1640	1634	5.243	3.347	0.093	−1.031
1630	1624	5.271	3.498	0.097	−1.012
1620	1614	5.299	3.635	0.101	−0.995

at Tg_{peak}) and thereby obtain a set of viscosity data, as a function of redox state, for these supercooled liquids immediately above Tg, shown in Fig. 7.

This viscosity-temperature data set is compared with that from the very high temperature superliquidus data set in Fig. 6 where the two data sets are fit using a single viscosity-temperature relationship. The influence of redox on this relationship is shown in Fig. 8 to be small but measurable.

4. Discussion

Comparison of the redox effect of Fe on the viscosity of pyrolite with all available data from the literature leads to the following conclusions.

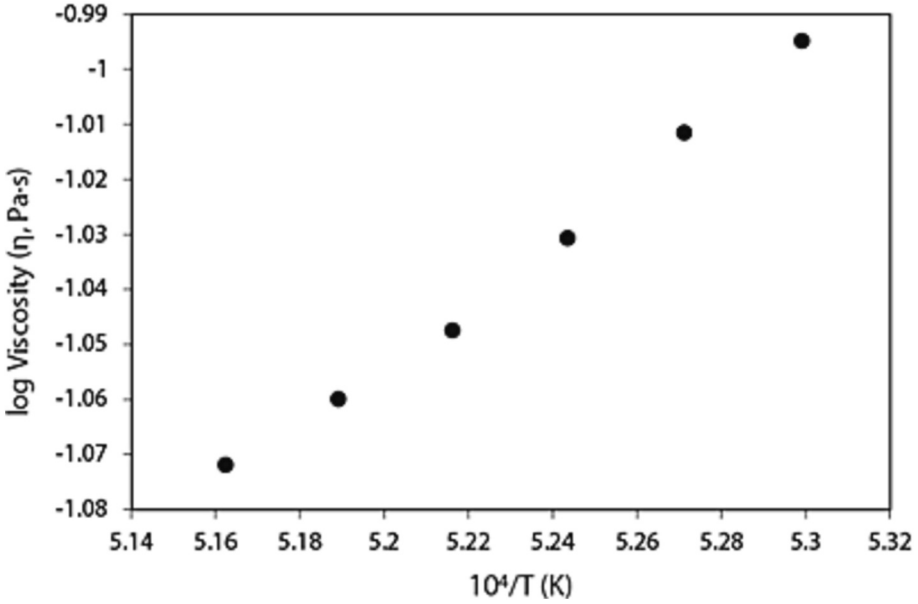

Fig. 6. Superliquidus viscosity vs reciprocal absolute temperature.

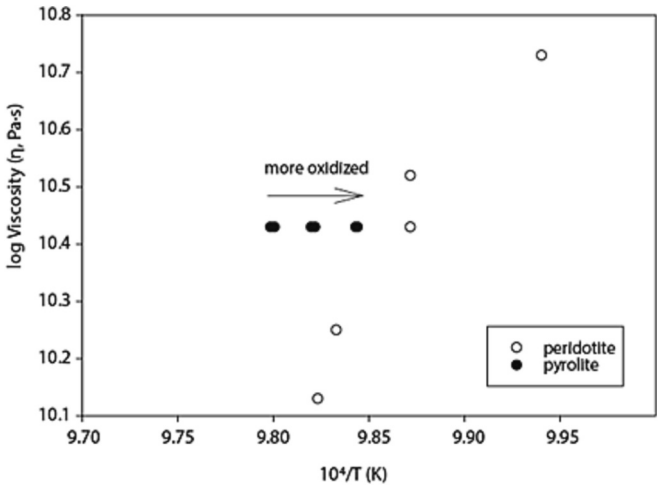

Fig. 7. Calorimetrically-derived low temperature viscosity of pyrolite versus the Balmuccia peridotite (Dingwell et al., 2004) as a function of the reciprocal absolute temperature.

In contrast to the clear positive effect of oxidation on viscosity (higher fO_2 increases viscosity), determined for alkali and alkaline earth silicate melts of higher silica content, pyrolite shows an opposite trend, i.e., decreasing viscosity with more oxidised redox states (increasing $Fe^{3+}/\Sigma Fe$ ratios). The investigation of fayalite-based slags (Kaiura et al., 1977) however, observed a negative redox dependent trend as seen here. The measured increase in Tg temperatures with increasing depolymerisation (higher NBO/T ratios) shown here, is also contrasting with the positive effect of increasing polymerisation on Tg, namely that more polymerised melts have higher Tg temperatures.

Thus, there would appear to be a basicity-dependent behaviour of silicate melt redox-viscosity relations going from a positive effect at high silica to a negative effect at low silica content (a decrease in viscosity upon higher fO_2 conditions). More comprehensive investigations of the structural roles of ferrous and ferric iron across this range might shed light on the compositional basis for this redox viscometry inversion.

5. Concluding remark

In contrast with the evidence of a positive redox effect of Fe on melt viscosity of most geological melts and their analogues, pyrolite shows a negative effect, i.e., higher iron redox states resulted in lower viscosity. Data from silica-poor slag systems confirm a negative effect similar to that observed here. The structural origins of this basicity-dependent effect remain unclear and require further work.

We conclude from the magnitude of the redox effect observed in this study that the effect of the oxidation state of iron on the viscosity of molten planetary interiors will be minor.

CRediT authorship contribution statement

Ana S. Casas: Conceptualization, Methodology, Validation, Investigation, Writing – review & editing, Visualization, Supervision. **Kai-Uwe Hess:** Conceptualization, Methodology, Validation, Writing – review & editing, Visualization, Investigation, Formal analysis. **James Badro:** Conceptualization, Resources, Methodology, Investigation, Writing – review & editing. **Michael Eitel:** Methodology, Investigation. **Donald B. Dingwell:** Conceptualization, Methodology, Validation, Investigation, Writing – original draft, Writing – review & editing, Visualization, Supervision, Funding acquisition.

Declaration of Competing Interest

The authors declare that they have no known competing financial interests or personal relationships that could have appeared to influence the work reported in this paper.

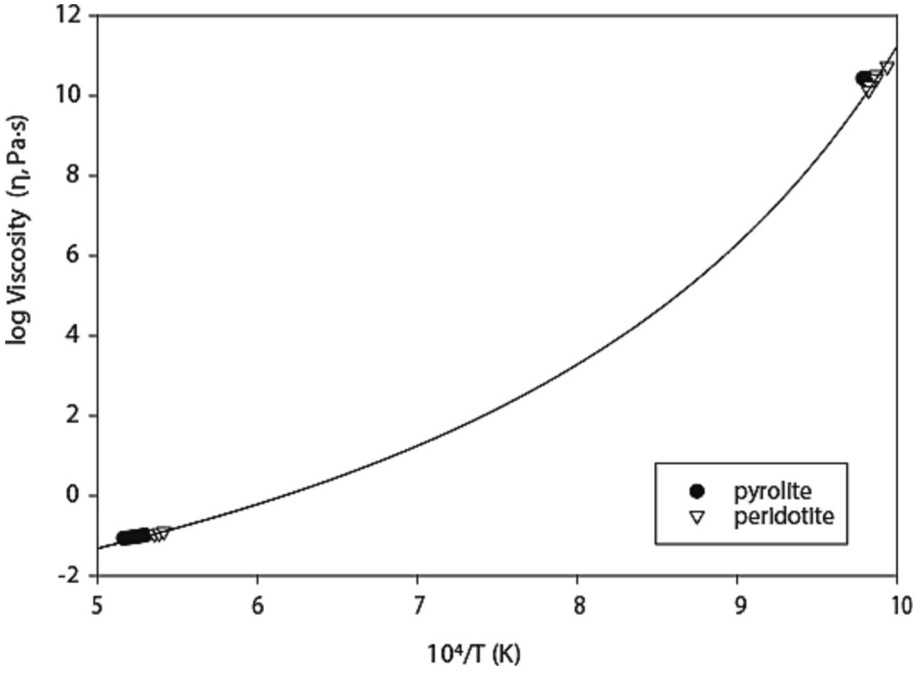

Fig. 8. Viscosities of peridotite and pyrolite melts, fitted using the VFT equation from Dingwell et al. (2004).

Data availability

Data will be made available on request.

Acknowledgements

DBD and ACR acknowledge the support of European Research Council - ADG 2018 Grant 834225 (EAVESDROP), ASC acknowledges the support of the Australian Research Council - Discovery Project Grant (DP200100406).

Appendix A. Supplementary data

Supplementary data to this article can be found online at https://doi.org/10.1016/j.chemgeo.2023.121816.

References

Dingwell, D.B., 1986. Viscosity-temperature relationships in the system Na2Si2O5-Na2Al4O5. Geochim. Cosmochim. Acta 50, 1261–1265. https://doi.org/10.1016/0016-7037(86)90409-6.

Dingwell, D.B., 1991. Redox viscometry of some Fe-bearing silicate melts. Am. Mineral. 76 (9–10), 1560–1562.

Dingwell, D., 1995. Chapter 2. Relaxation in silicate melts: Some applications. In: Stebbins, J., McMillan, P., Dingwell, D. (Eds.), Structure, Dynamics, and Properties of Silicate Melts. De Gruyter, Berlin, Boston, pp. 21–66. https://doi.org/10.1515/9781501509384-004.

Dingwell, D.B., Brearley, M., 1988. Melt densities in the CaO-FeO-Fe2O3-SiO2 system and the compositional dependence of the partial molar volume of ferric iron in silicate melts. Geochim. Cosmochim. Acta 52, 2815–2825. https://doi.org/10.1016/0016-7037(88)90149-4.

Dingwell, D.B., Virgo, D., 1987. The effect of oxidation state on the viscosity of melts in the system Na2O–FeO–Fe2O3–SiO2. Geochim. Cosmochim. Acta 51, 195–205. https://doi.org/10.1016/0016-7037(87)90231-6.

Dingwell, D.B., Virgo, D., 1988. Viscosities of melts in the Na2O-FeO-Fe2O3-SiO2 system and factors controlling relative viscosities of fully polymerized silicate melts. Geochim. Cosmochim. Acta 52, 395–403. https://doi.org/10.1016/0016-7037(88)90095-6.

Dingwell, D.B., Webb, S.L., 1990. Relaxation in silicate melts. Eur. J. Mineral. 2, 427–449. https://doi.org/10.1127/ejm/2/4/0427.

Dingwell, D.B., Brearley, M., Dickinson, J.J.E., 1988. Melt densities in the Na2O-FeO-Fe2O3-SiO2 system and the partial molar volume of tetrahedrally-coordinated ferric iron in silicate melts. Geochim. Cosmochim. Acta 52, 2467–2475. https://doi.org/10.1016/0016-7037(88)90305-5.

Dingwell, D.B., Courtial, P., Giordano, D., Nichols, A.R.L., 2004. Viscosity of peridotite liquid. Earth Planet. Sci. Lett. 226 (1–2), 127–138. https://doi.org/10.1016/j.epsl.2004.07.017.

Ferry, J.D., 1980. Viscoelastic Properties of Polymers, 3d ed. Wiley, New York (ISBN 0471048941.).

Green, D.H., 1989. Pyrolite. In: Petrology. Encyclopedia of Earth Science. Springer, Boston, MA. https://doi.org/10.1007/0-387-30845-8_205.

Kaiura, G.H., Toguri, J.M., Marchant, G., 1977. Viscosity of Fayalite-Based slags. Can. Metall. Q. 16 (1), 156–160. https://doi.org/10.1179/cmq.1977.16.1.156.

Lange, R.L., Carmichael, I.S.E., 1990. Thermodynamic properties of silicate liquids with emphasis on density, thermal expansion and compressibility. Rev. Mineral. Geochem. 24, 25–64.

Matsukage, K., Kawasaki, T., 2014. Hydrous origin of the continental cratonic mantle. Earth Planet. Sp. 66, 29. https://doi.org/10.1186/1880-5981-66-29.

Ringwood, A.E., 1962. A model for the upper mantle. J. Geophys. Res. 67 (2), 857–867. https://doi.org/10.1029/JZ067i002p00857.

Rongzhi, Li, 2000. Time-temperature superposition method for glass transition temperature of plastic materials. Mater. Sci. Eng. A 278, 36–45. https://doi.org/10.1016/S0921-5093(99)00602-4.

Shapiro, L., Brannock, W.W., 1956. Rapid Analysis of Silicate Rocks. Nature 178, 70–71. https://doi.org/10.3133/cir165.

Stevenson, R., Dingwell, D.B., Webb, S.L., Bagdassarov, N.L., 1995. The equivalence of enthalpy and shear relaxation in rhyolitic obsidians and quantification of the liquid–glass transition in volcanic processes. J. Volcanol. Geotherm. Res. 68, 297–306. https://doi.org/10.1016/0377-0273(95)00015-1.

Takahashi, E., Shimazaki, T., Tsuzaki, Y., Yoshida, H., 1993. Melting study of a peridotite KLB-1 to 6.5 GPa, and the origin of basaltic magmas. Philos. Trans. Royal Soc. London. Series A: Phys. Eng. Sci. 342, 105–120. https://doi.org/10.1098/rsta.1993.0008.

Weidner, D.J., 1985. A mineral physics test of a pyrolite mantle. Geophys. Res. Lett. 12, 417–420. https://doi.org/10.1029/GL012i007p00417.